Positron Generation and Acceleration in a Self-Organized Photon Collider Enabled by an Ultraintense Laser Pulse

K. Sugimoto,[1,2] Y. He,[3] N. Iwata,[2,4] I-L. Yeh,[5] K. Tangtartharakul,[3] A. Arefiev,[3] and Y. Sentoku[2]

[1]*Department of Physics, Graduate School of Science, Osaka University, 1-1 Machikanecho, Toyonaka, Osaka 560-0043, Japan*
[2]*Institute of Laser Engineering, Osaka University, 2-6 Yamadaoka, Suita, Osaka 565-0871, Japan*
[3]*Department of Mechanical and Aerospace Engineering, University of California at San Diego, La Jolla, California 92093, USA*
[4]*Institute for Advanced Co-Creation Studies, Osaka University, 1-1 Yamadaoka, Suita, Osaka 565-0871, Japan*
[5]*Department of Physics, University of California at San Diego, La Jolla, California 92093, USA*

We discovered a simple regime where a near-critical plasma irradiated by a laser of experimentally available intensity can self-organize to produce positrons and accelerate them to ultrarelativistic energies. The laser pulse piles up electrons at its leading edge, producing a strong longitudinal plasma electric field. The field creates a moving gamma-ray collider that generates positrons via the linear Breit-Wheeler process— annihilation of two gamma rays into an electron-positron pair. At the same time, the plasma field, rather than the laser, serves as an accelerator for the positrons. The discovery of positron acceleration was enabled by a first-of-its-kind kinetic simulation that generates pairs via photon-photon collisions. Using available laser intensities of 10^{22} W/cm^2, the discovered regime can generate a GeV positron beam with a divergence angle of around $10°$ and a total charge of 0.1 pC. The result paves the way to experimental observation of the linear Breit-Wheeler process and to applications requiring positron beams.

In astrophysics, creation of matter from light is ubiquitous, playing an important role for various astrophysical objects (e.g., see Refs. [1–5]). The advent of ultra-high-intensity laser facilities [6–8] promises to enable, for the first time, creation of electron-positron pairs from light alone on a macroscopic scale in the laboratory. If successfully implemented, this capability will open a new area of QED research [9–11] and enable laboratory studies of astrophysically relevant electron-positron plasmas [12]. The ability to generate positrons by a laser is also likely to impact the research on laser-driven positron acceleration. Currently, positrons are produced by an external source, and the focus is on finding augmented configurations that facilitate positron acceleration [13–16].

In the context of pair production from light alone, it is important to distinguish between the nonlinear [17] and linear [18] Breit-Wheeler (BW) processes. The nonlinear BW or the multiphoton process is the decay of a γ ray propagating through a laser pulse into a pair. The decay involves multiple coherent optical photons. Thus, many pairs via the nonlinear BW process [19–25] require a laser intensity in excess of 10^{23} W/cm^2. The linear BW or two-photon process is the annihilation of two energetic γ rays that leads to pair production. The two-photon process has no laser intensity requirement, but it does require a dense population of energetic γ rays to overcome the smallness of the cross section, $\sigma_{\gamma\gamma} \sim 10^{-25}$ cm^2, and the energy threshold. A laser-irradiated plasma can efficiently generate a

γ-ray beam [26–28], so colliding two such beams (produced by two different lasers) in vacuum is a possible approach to produce pairs [29,30]. The inherent γ-ray beam divergence requires the targets generating γ rays to be close to each other and makes experimental implementation challenging. A conceptually different approach is to generate and collide γ-ray beams inside one target [31]. This approach not only allows us to overcome the divergence and thus boost the pair yield [31], but, more importantly, it offers an unexplored opportunity to accelerate the linear BW positrons. If the positrons can be accelerated and collimated, then this would facilitate their detection, making a first laboratory observation of the linear BW process possible; it would also enable their use for applications like positron annihilation lifetime spectroscopy [32,33].

In this Letter, we present a simple but previously unknown regime where a dense plasma irradiated by a laser of experimentally achievable intensity self-organizes to produce positrons from light alone and accelerate them to ultrarelativistic energies. The laser pulse piles electrons up at its leading edge, producing a strong longitudinal plasma electric field that moves with the pulse. The field creates a moving γ-ray collider that generates positrons via the linear BW process and, at the same time, serves as an accelerator for the produced positrons. The discovery of the new positron acceleration mechanism and the synergistic interplay between the photon collider and the plasma accelerator was enabled by a first-of-its-kind kinetic

simulation that generates pairs via photon-photon collisions. This Letter builds on an important observation based on postprocessed photon data that a single laser pulse can generate a colliding population of γ rays in a dense structured plasma [34]. We find that the linear BW process produces about 10^7 pairs at 3×10^{22} W/cm^2, whereas the nonlinear BW process produces no pairs at all. About 10% of the positrons experience the forward acceleration and form a GeV beam with a divergence angle of 10°. The advantage of our regime is that it uses a simple setup and requires only a single laser with intensity already accessible at ELI [35] and CoReLS [36].

The laser-plasma interaction is self-consistently simulated in 2D-3V with the PIC code PICLS [37], which includes a radiation transport module [38,39] for energetic photons emitted via synchrotron radiation [40] and bremsstrahlung [41]. We have developed a module for simulating the linear BW process (see Supplemental Material [42]), making PICLS the first PIC code capable of generating linear BW pairs during the laser-plasma interaction and thus suitable for studies of positron dynamics. In our setup, a 25-fs, 3×10^{22} W/cm^2 laser pulse irradiates a dense uniform carbon plasma (see Supplemental Materials for simulation parameters). We normalize all electric fields $\boldsymbol{E}$ and use a dimensionless quantity $\boldsymbol{a} = |e|\boldsymbol{E}/m_e c \omega_0$ instead, where e and m_e are the electron charge and mass, c is the speed of light, and ω_0 is the laser frequency corresponding to vacuum wavelength $\lambda = 0.8$ μm. The laser amplitude is $a_L = 120$. This laser makes electrons ultrarelativistic and renders a plasma with electron density n_e less than $\gamma_L n_c \sim a_L n_c$ transparent, where $\gamma_L \equiv \sqrt{1 + a_L^2/2}$ is the electron Lorentz factor for ponderomotive energy [43] and $n_c = m_e \omega_0^2/4\pi e^2$ is the classical critical density. In our main simulation, the initial electron density is $n_{e0} = 2.8 n_c \ll a_L n_c$, so the laser easily propagates into the plasma.

Figure 1 illustrates key aspects of the laser-plasma interaction. All snapshots are taken when the laser pulse reaches $x = 30$ μm. The corresponding time is $t = 117$ fs, with $t = 0$ fs being the time when the pulse reaches the target. Figure 1(a) shows the normalized transverse electric field a_y that is dominated by the field of the laser. Because of the relativistic self-focusing, the beam remains tightly focused after having traveled a distance greater than the Rayleigh length ($l_R = \pi w_0^2/\lambda \simeq 25$ μm for a focal spot with radius $w_0 = 2.5$ μm). The dashed curves mark the expected beam waist in the absence of the target. The self-focusing also increases the laser amplitude to $a_y = 150$. The beam becomes fully depleted after it propagates 70 μm into the plasma. The profiles of the electron density and generated azimuthal magnetic field are shown in Figs. 1(b) and 1(c). Transverse electron expulsion by the ponderomotive force produces a density pileup ($n_e \sim 10 n_c$) at the periphery of the beam, which helps guide the laser. The electrons remaining in the beam accelerate forward in the laser field and form a longitudinal current. The current generates a
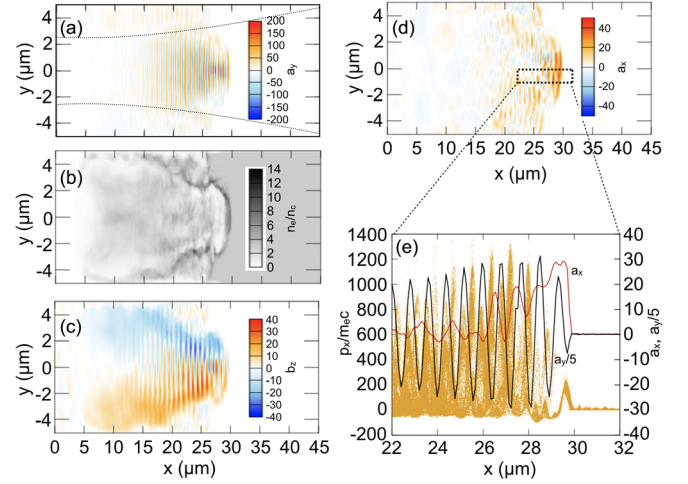

FIG. 1. Laser interaction with a dense plasma. (a) Normalized transverse electric field a_y. Dashed lines indicate the beam waist in the absence of the plasma. (b) Electron density. (c) Normalized magnetic field b_z averaged over one laser period. (d) Normalized longitudinal electric field a_x. (e) Electron distribution in the x-p_x plane, and a_x and a_y in the vicinity of the pulse front [dashed rectangle in (d)]. The electric fields a_x and a_y in (e) are averaged over $|y| \leq 0.5$ μm. The snapshots in (a)–(e) are taken at $t = 117$ fs.

strong quasistatic magnetic field B_z [28] whose peak strength is 30% of that for the laser magnetic field. Figure 1(c) shows the field profile while providing an additional figure of merit $b_z = \omega_c/\omega_0$, where $\omega_c = |e|B_z/m_e c$ is the cyclotron frequency.

The B field plays a key role in generating forward-directed γ rays. It transversely confines the electrons that are accelerated and pushed forward by the laser. The B field defects electrons forward instead of causing the conventional rotation, and the deflections change the orientation of the transverse velocity $v_\perp$ with respect to $E_\perp$ of the laser. If their frequency is comparable to the Doppler-shifted frequency of the laser, then $v_\perp$ remains antiparallel to $E_\perp$ as the laser field and the electron oscillate. This mechanism of direct laser acceleration assisted by the plasma B field [44] produces about 500 MeV electrons with a forward momentum of 1000 $m_e c$. They are located in Fig. 1(e) at 22 μm $\leq x \leq 28$ μm. The deflections of the electrons by the magnetic field have another important effect—they cause the electrons to emit MeV γ rays in the direction of laser propagation [28,30,45].

Because of the high plasma density, the laser also generates a strong longitudinal plasma electric field that is essential for the production of backward-directed γ rays. This is a charge-separation field that arises as the leading edge of the laser pulse sweeps up plasma electrons. Its peak amplitude is 25% of a_y, and it dominates over the oscillating longitudinal field of the laser. The positive plasma field is clearly visible in Fig. 1(d) at $x \approx 29.5$ μm. After initial forward acceleration to $p_x \sim 200\, m_e c$, the electrons swept
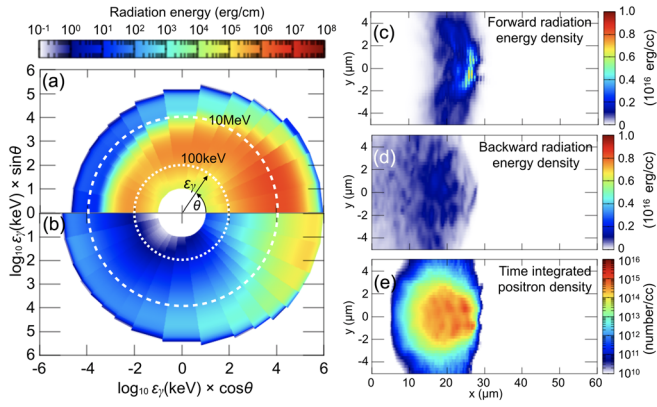
FIG. 2. Self-organized photon collider. (a) Angular distribution of the synchrotron photons and (b) that of the bremsstrahlung photons in the region with $22~\mu m \leq x \leq 27.5~\mu m$ and $|y| \leq 1~\mu m$. The radius is $\log_{10}\epsilon_\gamma[\text{keV}]$. The dashed circles are $\epsilon_\gamma = 100$ keV and 10 MeV. (c) Energy density of forward emitted photons via synchrotron emission and (d) that of backward emitted photons. (e) Time-integrated number density of the linear BW pair production events. The snapshots in (a)–(e) are taken at $t = 117$ fs.

up by the leading edge of the laser pulse slow down under the influence of a_x and then reaccelerate in the backward direction to $p_x \sim -100~m_e c$. These electrons emit backward-directed photons. In contrast to the forward-moving electrons, the emission is induced by the laser field [46], which is much stronger than the plasma magnetic field. This makes the emission more efficient, causing the electrons to quickly lose a large portion of their energy, as seen in Fig. 1(e) at $x > 28~\mu m$. The emission process accompanies laser propagation since the population of backward-moving electrons is constantly replenished by a_x, which is moving forward with the laser pulse.

The photons generated through synchrotron emission form a moving γ-ray collider, with Figs. 2(c) and 2(d) showing the energy density of the forward- and backward-moving photons. Figure 2(a) shows the photon spectrum versus the polar angle θ in the region where the two populations overlap. The bremsstrahlung that plays a secondary role is included for completeness. The synchrotron emission converts 40% of the laser energy into photons over the entire simulation (vs 2% for bremsstrahlung). The linear BW process has a threshold of $\epsilon_{\gamma 1}\epsilon_{\gamma 2} > m_e^2 c^4 \approx 0.26~\text{MeV}^2$, where $\epsilon_{\gamma 1,2}$ are the energies of colliding photons. Therefore, linear BW pairs are mainly produced by forward-moving photons with $0.5~\text{MeV} \lesssim \epsilon_\gamma \lesssim 100$ MeV colliding with backward-moving photons with $10~\text{keV} \lesssim \epsilon_\gamma \lesssim 1$ MeV. The photon densities in these two groups are comparable, with $n_\gamma \sim 10^{22}~\text{cm}^{-3}$. The probability for a backward-moving photon to produce a pair is $\sigma_{\gamma\gamma}n_\gamma l \sim 10^{-6}$, where $l \sim 10~\mu m$ is the length of the forward-moving photon cloud. The total number of backward photons is $n_\gamma SL \sim 10^{13}$, where $L \approx 70~\mu m$ is the laser depletion length and $S \approx 25~\mu m^2$ is the cross section of the
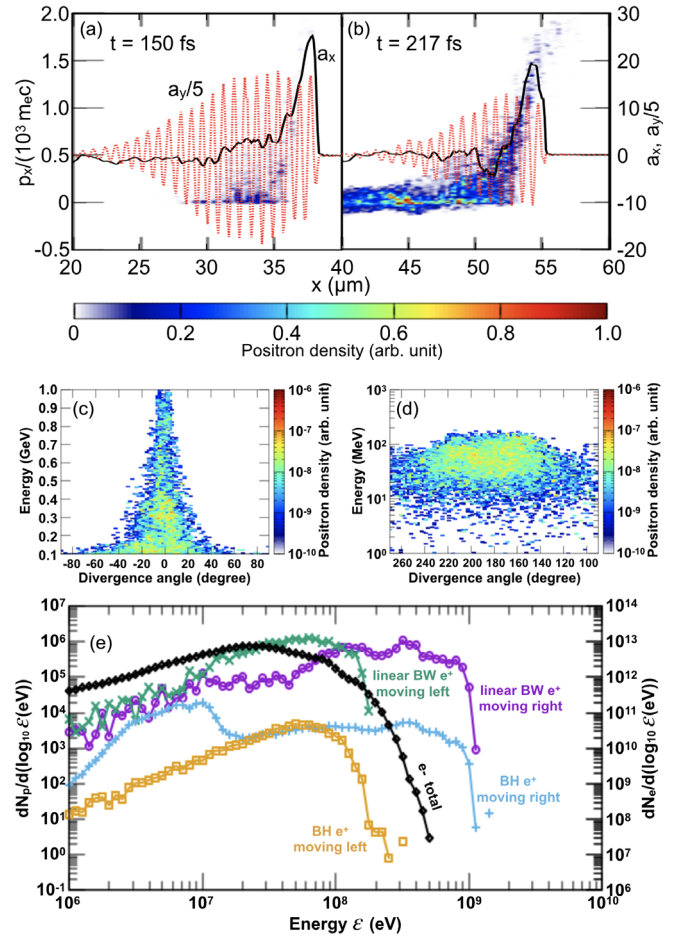

FIG. 3. Laser-driven positron accelerator. (a),(b) Positron distribution in (x, p_x) space for $|y| \leq 2~\mu m$ and electric-field profiles at $t = 150$ fs and 217 fs. The fields are averaged over $|y| \leq 2~\mu m$. (c) Energy vs divergence angle of forward-moving positrons at $t = 317$ fs and (d) that of backward-moving positrons. (e) Energy spectra at $t = 317$ fs of positrons produced via the linear BW process and via the BH process, and electrons. The third dimension is set to 5 μm to evaluate the number of particles.

cloud, assuming the length in the third dimension is the laser spot diameter. The predicted pair yield is 10^7, which matches the yield evaluated using the developed module for the linear BW process [34]. A similar module implemented by us in the PIC code EPOCH [47], which has a different approach for treating emitted photons, produced a comparable yield. A time-integrated density of the pair-production events is shown in Fig. 2(e).

The γ-ray collider is moving with the laser, continuously producing positrons with a mildly relativistic momentum $p \sim m_e c$ within the laser pulse [see Fig. 3(a)]. The positron dynamics is strongly influenced by the laser and plasma fields, with two distinct populations emerging over time: forward-moving positrons whose energies reach 1 GeV and backward-moving positrons whose energies reach 100 MeV. Figures 3(c) and 3(d) show terminal positron distributions in the energy-angle space for the forward and

backward positrons. Figure 3(e) shows the electron and positron energy spectra, distinguishing the linear BW and Bethe-Heitler (see Supplemental Material [42]) positrons to emphasize the dominant role of the linear BW process. A striking feature of Fig. 3(e) is that the peak energy of forward positrons exceeds the peak energy of forward electrons by a factor of 2. The electrons gain their energy from the laser via the direct laser acceleration assisted by the plasma magnetic field [44], but the positrons are not able to do this because they are positively charged. The plasma magnetic field deflects positrons backward rather than forward, which causes the formation of the backward positron population.

We tracked the energetic forward-moving positrons and found that they gain most of their energy (80%) from the strong forward-moving longitudinal plasma electric field, thus discovering a new positron acceleration mechanism. Figure 3(b) confirms that the energetic positrons are surfing with the spike in a_x. The positrons continue accelerating until they overtake the laser pulse or leave the acceleration region in the lateral direction. The acceleration by a_x only works for positrons, whereas the same field pulls plasma electrons backward, creating the backward emission that contributes to the photon collider.

The discovered acceleration mechanism produces 10^6 or 0.1 pC of positrons with energies above 100 MeV and an average divergence angle $|\theta| \sim 10°$. The high plasma density is not only important for generating strong a_x needed for positron acceleration (no a_x spike is produced at subcritical densities [25]), but it is also crucial for achieving a high number of accelerated positrons. Positrons must catch up with a_x to experience the acceleration, but this is hard to achieve if a_x, whose speed is u, moves too fast. In a low density plasma, u is close to the group velocity $v_g/c \approx \sqrt{1 - n_e/\gamma_L n_c}$ [48]. In a dense plasma, u is lower than v_g due to laser depletion, which enables more positrons to experience acceleration. In our case, $u/c \approx 0.8$, but $v_g/c \approx 0.98$. Only relativistic positrons with $v_x \approx c \cos\theta > u$ are able to catch up with a_x. We have $v_x \approx c \cos\theta > u$ for $|\theta| \leq 37°$, whereas $v_x \approx c \cos\theta > v_g$ for $|\theta| \leq 11°$. The 20% reduction in u compared to v_g increases the range of θ by a factor of 3 and thus significantly increases the number of positrons that can catch up with a_x.

To examine the impact of the plasma density n_{e0} on the strength of a_x and the positron energy gain, we performed extra simulations with $n_{e0}/n_c = 0.5, 1.0, 1.75$, and 5.6. Figures 4(a) and 4(b) show a_x at the leading edge of the pulse and the energy gain by forward-moving positrons versus n_{e0}. We average a_x over y at the time when the laser peak intensity reaches the pulse leading edge to obtain the values in Fig. 4(a). The energies in Fig. 4(b) were averaged over the top 5%, 10%, and 20% of the positron spectrum to confirm the trend. The discovered regime is robust and can be achieved over a wide range of plasma densities. For
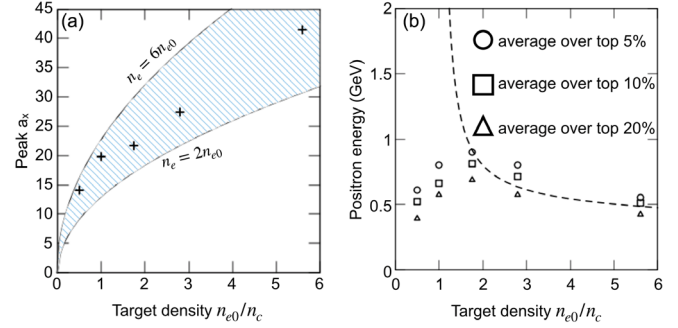

FIG. 4. (a) Normalized electric field a_x at the leading edge of the laser pulse as a function of target density. The shaded area is given by Eq. (1) for $2n_{e0} \leq n_e \leq 6n_{e0}$, $a_L = 120$, and $u = 0.8c$. (b) Positron energies averaged over the top 5%, 10%, and 20% of the positron spectra for different target densities. The dotted curve is $\Delta\epsilon_{e^+} = c\Delta p_{e^+}$ obtained from Eq. (2) for $a_L = 120$, $u = 0.8c$, and $n_e = 4n_{e0}$.

$n_c \leq n_{e0} \leq 5.6n_c$, the number of positrons with energies above 100 MeV and $|\theta| \lesssim 10°$ is consistently about 10^6. At $n_{e0}/n_c = 0.5$, the speed of a_x is very close to c, which makes a_x too fast to effectively accelerate positrons that are originally only mildly relativistic.

We next use estimates for a_x and the positron energy gain to determine their scaling at high n_{e0}. The electron density pileup responsible for a_x is sustained due to force balance, $0 = F_p + F_s$, between the laser ponderomotive force $F_p = -m_e c^2 \nabla_x \gamma_L$ and $F_s = -a_x m_e c \omega_0$. We estimate that $\gamma_L/|\nabla_x \gamma_L| \simeq l_{\text{skin}}$, where $l_{\text{skin}} = \sqrt{\gamma_L} c/\omega_{pe}$ is the relativistic skin depth. Taking into account that $a_L \gg 1$, we obtain

$$a_x \simeq \sqrt{\gamma_L n_e/n_c}, \tag{1}$$

where n_e is the density of the electron pileup. The shaded area in Fig. 4(a) shows a_x from Eq. (1) for $a_L = 120$ and $2n_{e0} \leq n_e \leq 6n_{e0}$. The latter is the entire range of n_e observed in the simulations, with $n_e \approx 2n_{e0}$ for $n_{e0} = 5.6n_c$ and $n_e \approx 6n_{e0}$ for $n_{e0} = 0.5n_c$. The momentum gain Δp_{e^+} from a_x can be estimated by integrating the positron equation of motion $dp_{e^+}/dt \simeq m_e c \omega_0 \bar{a}_x$ over the acceleration time interval Δt_{acc}, where $\bar{a}_x = a_x/2$ is the average field amplitude in the acceleration region. The length of the region with positive a_x is the width of the electron pileup, l_{skin}, plus the length of the positively charged electron cavity, l_{cav}, formed behind the pulse leading edge. We estimate l_{cav} from the charge conservation: $(n_{e0} - n_c)l_{\text{cav}} = (n_e - n_{e0})l_{\text{skin}}$ for $n_{e0} > n_c$. The acceleration region is moving forward with velocity u while the positron velocity is v_x, so $\Delta t_{\text{acc}} \equiv (l_{\text{cav}} + l_{\text{skin}})/(v_x - u)$. Assuming an ultrarelativistic positron, we set $v_x \sim c$. After taking into account that $\gamma_L n_c \gg n_e$ for $a_L \gg 1$, we find that the positron momentum gain is

$$\Delta p_{e^+} \simeq \frac{\gamma_L m_e c}{2} \frac{1}{1 - u/c} \frac{n_e - n_c}{n_{e0} - n_c}. \tag{2}$$

Equation (2) gives $\Delta p_{e^+}/m_e c \simeq 1200$ for $n_{e0} = 2.8 n_c$, $a_L = 120$, $u = 0.8c$, and $n_e = 4 n_{e0}$, reproducing the significant positron momentum increase at the pulse leading edge seen in Fig. 3(b). The energy gain $\Delta\epsilon_{e^+} = c\Delta p_{e^+}$ obtained from Eq. (2) is shown in Fig. 4(b) with a dashed curve. For high densities, $\Delta\epsilon_{e^+}$ has a weak dependence on n_{e0} because the increase in a_x is counteracted by the reduction in the acceleration time caused by lower u.

In summary, we discovered a robust regime where a laser-irradiated plasma self-organizes to produce positrons and accelerate them. The GeV-level positron beam can be generated using just a single laser with an experimentally available intensity. The regime requires the use of a dense plasma that can create a strong longitudinal electric field via electron pileup. The field is crucial for creating the γ-ray collider and for accelerating positrons. The positron acceleration was discovered by a first-of-its-kind simulation code generating pairs via photon-photon collisions. This code has direct relevance to astrophysics research since correct treatment of secondary pairs is one of the main problems facing modern PIC simulations of pulsars [3,5]. The uniform density is a simplification and not a requirement. A simulation with n_e ramping up from 0.5 to $3n_c$ over 60 μm has a similar pair yield of 10^7. The 3D simulation with PICLS (see Supplemental Material) demonstrates the self-organization of the field structure, and the 3D EPOCH [47] simulation has a n_γ similar to that in our 2D simulations, confirming the robustness of the discussed phenomena. Lastly, our regime can be instrumental in gauging the focal intensity of multi-PW lasers. At 10^{21} W/cm^2, the positron yield is 5 orders of magnitude lower than at 10^{22} W/cm^2. Therefore, the presence of energetic positrons in the laser direction can be a confirmation of laser intensity exceeding 10^{22} W/cm^2.

[1] Z. Medin and D. Lai, Mon. Not. R. Astron. Soc. **406**, 1379 (2010).
[2] A. M. Beloborodov, Astrophys. J. **683**, L41 (2008).
[3] A. A. Philippov and A. Spitkovsky, Astrophys. J. **855**, 94 (2018).
[4] A. Y. Chen, D. Uzdensky, and J. Dexter, Astrophys. J. **944**, 173 (2023).
[5] H. Hakobyan, A. Philippov, and A. Spitkovsky, Astrophys. J. **943**, 105 (2023).
[6] C. N. Danson, C. Haefner, J. Bromage, T. Butcher, J.-C. F. Chanteloup, E. A. Chowdhury, A. Galvanauskas, L. A. Gizzi, J. Hein, D. I. Hillier et al., High Power Laser Sci. Eng. **7**, 1 (2019).
[7] K. Tanaka, K. Spohr, D. Balabanski, S. Balascuta, L. Capponi, M. Cernaianu, M. Cuciuc, A. Cucoanes, I. Dancus, A. Dhal et al., Matter Radiat. Extremes **5**, 024402 (2020).
[8] J. W. Yoon, C. Jeon, J. Shin, S. K. Lee, H. W. Lee, I. W. Choi, H. T. Kim, J. H. Sung, and C. H. Nam, Opt. Express **27**, 20412 (2019).
[9] A. Di Piazza, C. Müller, K. Z. Hatsagortsyan, and C. H. Keitel, Rev. Mod. Phys. **84**, 1177 (2012).
[10] A. Gonoskov, T. G. Blackburn, M. Marklund, and S. S. Bulanov, Rev. Mod. Phys. **94**, 045001 (2022).
[11] P. Zhang, S. S. Bulanov, D. Seipt, A. V. Arefiev, and A. G. R. Thomas, Phys. Plasmas **27**, 050601 (2020).
[12] A. Di Piazza, L. Willingale, and J. Zuegel, arXiv:2211.13187.
[13] S. Gessner, E. Adli, J. M. Allen, W. An, C. I. Clarke, C. E. Clayton, S. Corde, J. Delahaye, J. Frederico, S. Z. Green et al., Nat. Commun. **7**, 11898 (2016).
[14] S. Zhou, J. Hua, W. An, W. B. Mori, C. Joshi, J. Gao, and W. Lu, Phys. Rev. Lett. **127**, 174801 (2021).
[15] T. Silva, L. D. Amorim, M. C. Downer, M. J. Hogan, V. Yakimenko, R. Zgadzaj, and J. Vieira, Phys. Rev. Lett. **127**, 104801 (2021).
[16] J. Vieira and J. T. Mendonça, Phys. Rev. Lett. **112**, 215001 (2014).
[17] D. L. Burke, R. C. Field, G. Horton-Smith, J. E. Spencer, D. Walz, S. C. Berridge, W. M. Bugg, K. Shmakov, A. W. Weidemann, C. Bula et al., Phys. Rev. Lett. **79**, 1626 (1997).
[18] G. Breit and J. A. Wheeler, Phys. Rev. **46**, 1087 (1934).
[19] C. P. Ridgers, C. S. Brady, R. Duclous, J. G. Kirk, K. Bennett, T. D. Arber, A. P. L. Robinson, and A. R. Bell, Phys. Rev. Lett. **108**, 165006 (2012).
[20] M. Vranic, O. Klimo, G. Korn, and S. Weber, Sci. Rep. **8**, 4702 (2018).
[21] X.-L. Zhu, M. Chen, T.-P. Yu, S.-M. Weng, F. He, and Z.-M. Sheng, Matter Radiat. Extremes **4**, 014401 (2019).
[22] J.-X. Liu, T.-P. Yu, L.-Q. Cao, Y. Zhao, G.-B. Zhang, L. Ma, S. Qu, Y.-Y. Ma, F.-Q. Shao, and J. Zhao, Plasma Phys. Controlled Fusion **61**, 065014 (2019).
[23] J. Zhao, Y.-T. Hu, Y. Lu, H. Zhang, L.-X. Hu, X.-L. Zhu, Z.-M. Sheng, I. C. E. Turcu, A. Pukhov, F.-Q. Shao et al., Commun. Phys. **5**, 1 (2022).
[24] A. Mercuri-Baron, M. Grech, F. Niel, A. Grassi, M. Lobet, A. D. Piazza, and C. Riconda, New J. Phys. **23**, 085006 (2021).
[25] B. Martinez, B. Barbosa, and M. Vranic, Phys. Rev. Accel. Beams **26**, 011301 (2023).
[26] T. Nakamura, J. K. Koga, T. Z. Esirkepov, M. Kando, G. Korn, and S. V. Bulanov, Phys. Rev. Lett. **108**, 195001 (2012).
[27] L. L. Ji, A. Pukhov, I. Y. Kostyukov, B. F. Shen, and K. Akli, Phys. Rev. Lett. **112**, 145003 (2014).
[28] D. J. Stark, T. Toncian, and A. V. Arefiev, Phys. Rev. Lett. **116**, 185003 (2016).
[29] X. Ribeyre, E. d'Humières, O. Jansen, S. Jequier, V. T. Tikhonchuk, and M. Lobet, Phys. Rev. E **93**, 013201 (2016).

[30] T. Wang, X. Ribeyre, Z. Gong, O. Jansen, E. d'Humières, D. Stutman, T. Toncian, and A. Arefiev, Phys. Rev. Appl. **13,** 054024 (2020).

[31] Y. He, T. G. Blackburn, T. Toncian, and A. V. Arefiev, Commun. Phys. **4,** 139 (2021).

[32] T. L. Audet, A. Alejo, L. Calvin, M. H. Cunningham, G. R. Frazer, G. Nersisyan, M. Phipps, J. R. Warwick, G. Sarri, N. A. M. Hafz, C. Kamperidis, S. Li, and D. Papp, Phys. Rev. Accel. Beams **24,** 073402 (2021).

[33] R. R. Krause-Rehberg, *Positron Annihilation in Semiconductors: Defect Studies*, Springer Series in Solid-State Sciences Vol. 127 (Springer, Berlin, 1999).

[34] Y. He, I. Yeh, T. Blackburn, and A. Arefiev, New J. Phys. **23,** 115005 (2021).

[35] See https://eli-laser.eu.

[36] See https://corels.ibs.re.kr/html/corels_en.

[37] Y. Sentoku and A. J. Kemp, J. Comput. Phys. **227,** 6846 (2008).

[38] Y. Sentoku, I. Paraschiv, R. Royle, R. C. Mancini, and T. Johzaki, Phys. Rev. E **90,** 051102(R) (2014).

[39] R. Royle, Y. Sentoku, R. C. Mancini, I. Paraschiv, and T. Johzaki, Phys. Rev. E **95,** 063203 (2017).

[40] R. R. Pandit and Y. Sentoku, Phys. Plasmas **19,** 073304 (2012).

[41] Y. Sentoku, K. Mima, T. Taguchi, S. Miyamoto, and Y. Kishimoto, Phys. Plasmas **5,** 4366 (1998).

[42] See Supplemental Material at http://link.aps.org/supplemental/10.1103/PhysRevLett.131.065102, for 1) setup of 2D PIC simulations, 2) algorithm for computing the linear BW pair yield, 3) 3D PIC simulation of the self-organization of the field structure, and 4) comparison of the pair creation with the BH process.

[43] S. C. Wilks, W. L. Kruer, M. Tabak, and A. B. Langdon, Phys. Rev. Lett. **69,** 1383 (1992).

[44] Z. Gong, F. Mackenroth, T. Wang, X. Q. Yan, T. Toncian, A. V. Arefiev et al., Phys. Rev. E **102,** 013206 (2020).

[45] O. Jansen, T. Wang, D. J. Stark, E. d'Humières, T. Toncian, and A. Arefiev, Plasma Phys. Controlled Fusion **60,** 054006 (2018).

[46] J. Koga, Phys. Rev. E **70,** 046502 (2004).

[47] T. Arber, K. Bennett, C. Brady, A. Lawrence-Douglas, M. Ramsay, N. Sircombe, P. Gillies, R. Evans, H. Schmitz, A. Bell et al., Plasma Phys. Controlled Fusion **57,** 113001 (2015).

[48] Y. Sentoku, W. Kruer, M. Matsuoka, and A. Pukhov, Fusion Sci. Technol. **49,** 278 (2006).

Correction: The article identification number in Ref. [31] was incorrect and has been fixed. The reference now links to the intended article.